JACS
JOURNAL OF THE AMERICAN CHEMICAL SOCIETY
Communication
pubs.acs.org/JACS

Solar Hydrogen Generation by Nanoscale *p*−*n* Junction of *p*-type Molybdenum Disulfide/*n*-type Nitrogen-Doped Reduced Graphene Oxide

Fanke Meng,[†] Jiangtian Li,[†] Scott K. Cushing,[†,‡] Mingjia Zhi,[†] and Nianqiang Wu[†,*]

[†]Department of Mechanical and Aerospace Engineering, West Virginia University, Morgantown, West Virginia 26506-6106, United States

[‡]Department of Physics, West Virginia University, Morgantown, West Virginia 26506-6315, United States

Supporting Information

ABSTRACT: Molybdenum disulfide (MoS_2) is a promising candidate for solar hydrogen generation but it alone has negligible photocatalytic activity. In this work, 5−20 nm sized *p*-type MoS_2 nanoplatelets are deposited on the *n*-type nitrogen-doped reduced graphene oxide (*n*-rGO) nanosheets to form multiple nanoscale *p*−*n* junctions in each rGO nanosheet. The *p*-MoS_2/*n*-rGO heterostructure shows significant photocatalytic activity toward the hydrogen evolution reaction (HER) in the wavelength range from the ultraviolet light through the near-infrared light. The photoelectrochemical measurement shows that the *p*-MoS_2/*n*-rGO junction greatly enhances the charge generation and suppresses the charge recombination, which is responsible for enhancement of solar hydrogen generation. The *p*-MoS_2/*n*-rGO is an earth-abundant and environmentally benign photocatalyst for solar hydrogen generation.

Hydrogen is a green fuel that does not generate carbon dioxide during combustion, which plays an important role in meeting the growing energy needs of the world. It is of great interest to utilize solar energy to produce hydrogen from renewable resources such as water.[1−5] Currently precious metals such as Pt, Rh, and Pd are essential components in the catalysts for the hydrogen evolution reaction (HER). The high cost and scarcity of these precious metals counters the benefits gained from an otherwise environmentally sustainable energy source.[1,6,7] It is vital to find inexpensive, earth-abundant materials to replace precious metal catalysts for sustainable development. Molybdenum disulfide (MoS_2) is a nontoxic, environmentally friendly and abundant semiconductor with the potential to fill this void. MoS_2 is widely used as an electrocatalyst for HER.[1,8,9] MoS_2 alone has negligible photocatalytic activity despite the fact that bulk MoS_2 has an indirect absorbance edge at ∼1040 nm,[10] which seems ideal for solar light harvesting. It remains unclear why MoS_2 is effective as an electrocatalyst but inactive as a photocatalyst. However, when MoS_2 is combined with other cocatalysts it does exhibit photocatalytic activity toward HER.[11−16] For example, MoS_2 has shown photocatalytic activity when it was coupled with $Ru(bpy)_3^{2+}$-based photosensitizer molecules,[14] indicating that insufficient charge separation in MoS_2 may limit its photoactivity. Similarly, MoS_2 has been used as a cocatalyst with CdS.[11] Unfortunately CdS is toxic and unstable under photochemical reaction.

Graphene and reduced graphene oxide (rGO) have been incorporated with semiconductors to form heterostructures to improve the catalytic activity in either photocatalysis[17−26] or electrocatalysis.[8] For example, MoS_2 nanoparticles (NPs) supported on rGO have been proven to be active HER electrocatalysts.[8] Recently, Eosin Y dye and the MoS_2 NPs have been codeposited on the rGO nanosheets to form a photocatalyst.[26] However, the MoS_2-rGO system shows no photocatalytic activity in the absence of a photosensitizer (Eosin Y dye), which indicates that MoS_2 provides reaction sites for HER but it does not harvest solar energy. In the semiconductor-rGO composite photocatalysts reported previously, rGO was treated as a metallic support to allow conduction. It was always considered as a passive component that provided a channel for charge transport, not help with the charge generation.

MoS_2 has a layered S−Mo−S structure, which has extremely low conductivity between adjacent S−Mo−S layers,[1] leading to poor charge mobility. Bulk MoS_2 has poor catalytic activity toward HER. For nanosized MoS_2, the edges of the S−Mo−S layers are the active sites for HER activity.[27,28] Two strategies have been proposed to improve the HER catalytic activity of MoS_2:[1,29,30] (i) increase the number of active sites and (ii) promote the charge transport. In this paper, a thin nanoplatelet structure of MoS_2 will be fabricated to create a large percentage of edge sites. This nanoplatelet structure will also shorten the distance that photogenerated charge carriers diffuse to the reaction sites, lowering the charge recombination loss that usually occurs during volume diffusion. The nanoplatelet geometry will also increase the contact area with the rGO sheets as compared to the spherical particles that are only in point contact with rGO. The increased contact area will promote the charge transfer at the MoS_2/rGO interface. In addition, the rGO nanosheets will be doped with nitrogen to form a *n*-type semiconductor as a support to grow the *p*-type MoS_2 nanoplatelets, forming many nanoscale *p*−*n* junctions on each rGO nanosheet. The space charge layer created by the nanoscale *p*−*n* junctions will not only suppress the charge recombination but also enhance the photogeneration of electron−hole pairs. In this photocatalyst system, MoS_2 not only acts as a catalytic center

Received: May 14, 2013
Published: June 28, 2013

dx.doi.org/10.1021/ja404851s | *J. Am. Chem. Soc.* 2013, 135, 10286−10289

but also as a photocenter for absorbing solar light to generate charge carriers. As a result, the nanoscale $p-n$ junction increases the photocatalytic activity toward HER. Furthermore, no noble metals or toxic materials are used in the p-MoS_2/n-rGO photocatalyst. This work presents an effective method to improve the HER photocatalysis of semiconductors without sacrificing environmental sustainability by incorporating precious metals or toxic cocatalysts.

Three types of photocatalysts were synthesized in this study, that is, (i) the free-standing solitary MoS_2 nanoparticles, (ii) the MoS_2/rGO composite where the MoS_2 nanoplatelets were supported on the undoped rGO sheets, and (iii) the p-MoS_2/n-rGO junction composite where the p-type MoS_2 nanoplatelets were deposited on the n-type nitrogen-doped rGO semiconductor sheets. All three types of photocatalysts were synthesized with a hydrothermal method. The experimental details are seen in the Supporting Information (SI). The bare rGO had a smooth flat surface before deposition (Figure 1a).

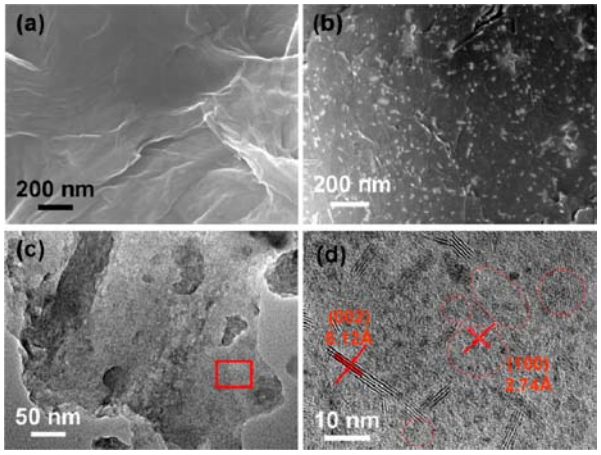

Figure 1. SEM images obtained from (a) the rGO sheets, (b) the p-MoS_2/n-rGO; (c) TEM image of the p-MoS_2/n-rGO, and (d) HRTEM image of the p-MoS_2/n-rGO from the area marked in the red square in image c.

Figure 1b shows that the MoS_2 nanoparticles were successfully grown on the nitrogen-doped rGO sheets. The MoS_2 nanoparticles were uniformly distributed on the n-rGO with a size of 5−20 nm. Before doping with nitrogen, the MoS_2/rGO composite (SI, Figure S1) showed similar morphology as the p-MoS_2/n-rGO junction composite in Figure 1c,d, which indicated the MoS_2 was not damaged in the nitrogen-doping process. In contrast, the bare MoS_2 without rGO had a "nanoball" structure composed of MoS_2 nanoplatelets with a lateral size of ~80 nm (SI, Figure S2). The results show that the rGO effectively restrained the aggregation of the MoS_2 nanoplatelets. The p-type MoS_2 had a hexagonal structure, as confirmed by the XRD pattern in SI, Figure S3. The broad peaks for the (002), (100), and (110) crystal planes at 14.4°, 32.7°, and 58.4° indicated that the nanostructured MoS_2 was crystalline. A broad peak at 24° resulted from the rGO.[26] Figure 1c shows a TEM image of the p-MoS_2/n-rGO. The marked area was enlarged for a HRTEM image in Figure 1d. The single-crystalline MoS_2 nanoparticles synthesized on the n-rGO sheet had a lattice spacing of 6.12 Å and 2.74 Å, corresponding to the (002) and (100) facets, respectively (JCPDS: 77-1716). The XPS spectra in Figure 2a and SI, Figure S4 confirmed the formation of rGO[31−33] and the successful nitrogen doping in the rGO sheets. The

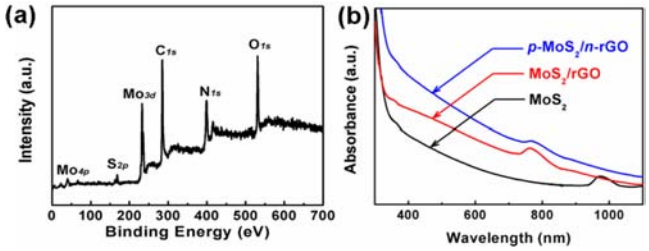

Figure 2. (a) XPS spectrum of the p-MoS_2/n-rGO, (b) UV−visible absorption spectra of the solitary MoS_2, the MoS_2/rGO, and the p-MoS_2/n-rGO.

doping concentration of N was estimated to be 6.4 atom % in the n-rGO sheets. The molar ratio of rGO to MoS_2 was 10.5:1 in the p-MoS_2/n-rGO.

The UV−visible spectrum in Figure 2b shows that solitary MoS_2 had an absorbance tail that stretched to 1020 nm, corresponding to the indirect band gap between Γ and the middle of the Brillouin zone between Γ and K.[34,35] For bulk MoS_2, the absorbance edge is typically cut off at 1040 nm.[10] In addition, solitary MoS_2 exhibited weak absorption at around 962 nm, and the MoS_2/rGO and p-MoS_2/n-rGO samples had the weak absorption at 781 and 786 nm, respectively. Similar phenomenon was also found in the nanosized MoS_2 particles reported previously.[10,36] The weak absorption peaks were due to the direct transition at the K point or to the contributions of excitonic transitions.[34,35]

For comparative studies, three types of particulate photocatalysts, including the solitary MoS_2, the MoS_2/rGO composite, and the p-MoS_2/n-rGO junction, were tested in the water/ethanol mixture solution under simulated solar light irradiation (Figure 3). Ethanol was a sacrificial reagent that acted as a hole-

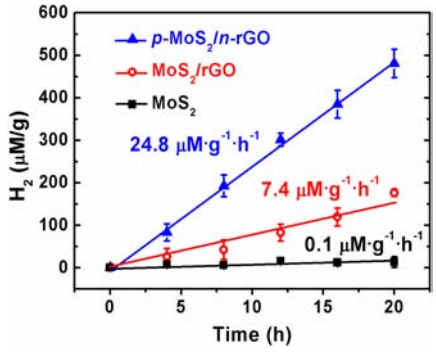

Figure 3. Hydrogen generated by the MoS_2, the MoS_2/rGO, and the p-MoS_2/n-rGO photocatalysts.

scavenger. MoS_2 alone showed negligible photocatalytic activity toward H_2 generation. Although the conduction band alignment of the bulk MoS_2 particles is not suitable for water reduction,[10,35] the quantum confinement of the nanosized MoS_2 makes it thermodynamically possible to reduce water to hydrogen. The solitary MoS_2 has the HER-active edges and absorption properties necessary for HER. However, the lack of activity indicates that either charge separation is extremely inefficient or the photogenerated charges cannot migrate to the HER-active edges. In contrast, the composite MoS_2/rGO, in which the MoS_2 nanoparticles were supported on the undoped rGO, showed evident photocatalytic activity with a hydrogen generation rate of 7.4 $\mu M \cdot g^{-1} \cdot h^{-1}$. Doping nitrogen into the rGO nanosheets led to

dx.doi.org/10.1021/ja404851s | J. Am. Chem. Soc. 2013, 135, 10286−10289

the formation of hundreds of $p-n$ junctions on each n-rGO sheets. As a result, the H_2 generation rate further increased to 24.8 $\mu M \cdot g^{-1} \cdot h^{-1}$. The surface area of the solitary MoS_2 was 134.3 m^2/g, which was even larger than that of the MoS_2/rGO (112.3 m^2/g) and the p-MoS_2/n-rGO (106.6 m^2/g), negating the surface area effects from explaining the difference in photoactivity. The improvement in photoactivity was solely due to the existence of the MoS_2/rGO heterostructure. Moreover, no hydrogen was generated by any of the samples in pure ethanol under the light irradiation after 10 h, which indicated that the hydrogen was generated from photocatalytic water splitting instead of ethanol reforming. The hydrogen generation experiments were repeated three cycles for each sample, which demonstrated the stable photocatalytic activity of the samples (SI, Figure S5). The photocatalytic H_2 generation rate of the p-MoS_2/n-rGO was relatively lower than the other materials reported previously,[11,26] which was due to much lower intensity of irradiation used in the present work. To measure the practical performance, the p-MoS_2/n-rGO sample was exposed to the natural sun light on our campus for H_2 generation (Table S1 and S2 in SI). The average hydrogen generation rate was measured to be 160.6 $\mu M \cdot g^{-1} \cdot h^{-1}$.

The three types of particulate photocatalysts were immobilized on fluorine tin oxide (FTO) substrates to form nanoparticle film photoelectrodes (see the experimental details in SI). The photoelectrochemical performance of the films was measured in a 1.0 M NaOH electrolyte solution using a three-electrode photoelectrochemical cell (PEC). To acquire the Mott−Schottky (M−S) plots, impedance spectroscopy was performed at an AC frequency of 10 kHz in the dark and under the simulated solar irradiation, respectively. Both the MoS_2 and the MoS_2/rGO photoelectrodes showed a negative slope for the M−S plots both in the dark and under light irradiation (SI, Figure S6), which indicated a p-type behavior.[37] The charge carrier densities in the solitary MoS_2 were measured to be 3.59×10^{14} cm^{-3} and 4.67×10^{15} cm^{-3} in the dark and light irradiation, respectively, while the charge carrier densities in MoS_2/rGO were measured to be 9.14×10^{16} cm^{-3} and 1.82×10^{17} cm^{-3} in the dark and light irradiation, respectively. It is well-known that the MoS_2 is a p-type semiconductor and the nitrogen-doped rGO is a n-type semiconductor.[1,38,39] When they were coupled to each other to form a heterostructure, a $p-n$ junction characteristic was observed in the M−S plot where an inverted "V-shape" was present (Figure 4a).[2] The donor densities in the p-MoS_2/n-rGO were 4.22×10^{18} cm^{-3} in the dark and 7.14×10^{18} cm^{-3} under light irradiation, respectively. The increased donor density in the p-MoS_2/n-rGO indicated that the nanoscale $p-n$ junction created a sufficient space charge layer to enhance the charge carrier creation under light irradiation.

The PEC performance was evaluated as shown in the current density (J)-potential (V) curve (Figure 4b). For independent MoS_2 or rGO, only a very small photocurrent was observed even at a potential of −0.5 V vs Reversible Hydrogen Electrode (RHE). Under light irradiation, the onset potential for photocurrent generation for the MoS_2/rGO was −0.10 V *vs* RHE; and the onset potential for the p-MoS_2/n-rGO shifted to 0.05 V vs RHE. The onset potential for photocurrent generation typically reflects the catalytic activity of the photoelectrode.[40,41] The shift of onset potential indicated that the formation of the $p-n$ junction improved the catalytic activity toward HER. At a high potential, the photocurrent density reflects the HER rate, which is controlled by the delivery rate of electrons to the electrode/electrolyte interface. Figure 4b shows that the

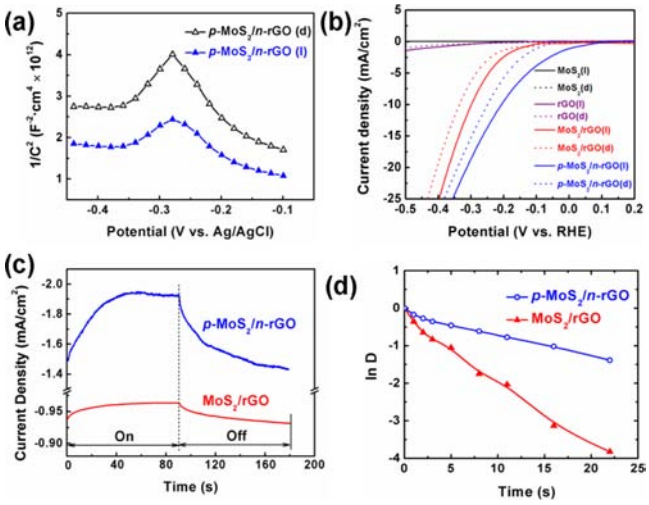

Figure 4. (a) Mott−Schottky plots of the p-MoS_2/n-rGO in dark (d) and under light (l) irradiation; (b) $J-V$ curves of the various catalysts and the bare rGO in dark (d) and under light (l) irradiation; (c) On−off $J-t$ curves of the MoS_2/rGO and the p-MoS_2/n-rGO under light (On) in dark (Off) at −0.1 V vs RHE; (d) normalized plots of the photocurrent−time dependence for the MoS_2/rGO and the p-MoS_2/n-rGO.

photocurrent density was greatly enhanced after MoS_2 was coupled to the undoped rGO; and the p-MoS_2/n-rGO junction further increased the photocurrent density. This indicates that the $p-n$ junction facilitated the charge generation and migration, as well as suppressed the charge recombination.[42,43] The photoelectrochemical activity of the photoelectrode as a function of wavelength was quantitatively investigated by the incident photon-to-electron conversion efficiency (IPCE) curve (SI, Figure S7), which was measured at a bias of −0.1 V vs RHE. It is noted that the p-MoS_2/n-rGO junction showed photocatalytic activity toward H_2 generation in a wide spectral range from the ultraviolet light through the near-infrared light region. Above 780 nm, the photoresponse of both the MoS_2/rGO composite and the p-MoS_2/n-rGO junction dropped to zero, which was in agreement with the light absorption behavior. At 400 nm, the solitary MoS_2 showed negligible photoresponse while the IPCE values of the MoS_2/rGO and the p-MoS_2/n-rGO were 2.8% and 13.6%, respectively. In the MoS_2/rGO composite, the rGO increases the energy conversion efficiency as a passive charge extraction layer. When a nanoscale $p-n$ junction is formed, the space charge layer creates a built-in electric field and separates the electrons and holes upon light illumination. Hence the $p-n$ junction changes the role of rGO from passive to active, further enhancing the charge separation.

The hydrogen evolution rate is strongly dependent on the charge recombination rate. The transient photocurrent (chronoamperometric) curve was acquired to investigate the charge recombination behavior (Figure 4c). However, no photocurrent was detected for solitary MoS_2 in SI, Figure S8. A normalized parameter (D) was derived from the transient photocurrent curve to quantitatively determine the charge recombination behavior,[44]

$$D = (I_t - I_{st})/(I_{in} - I_{st}) \quad (1)$$

where I_t, I_{st}, and I_{in} are the time-dependent, the steady-state, and the initial photocurrents, respectively. Figure 4d shows the normalized plots of ln $D-t$. The transient time constant (τ) is defined as the time when ln $D = -1$.[43] τ was estimated to be 4.4 s

dx.doi.org/10.1021/ja404851s | J. Am. Chem. Soc. 2013, 135, 10286−10289

for the MoS_2/rGO and 16.2 s for the *p*-MoS_2/*n*-rGO, which confirmed the suppression of charge recombination due to the space charge layer of the nanoscale *p*−*n* junction.

In summary, three types of photocatalysts, including solitary MoS_2, the *p*-MoS_2/undoped-rGO composite and the *p*-MoS_2/*n*-rGO junction were tested. The solitary MoS_2 nanoparticles showed little photocatalytic activity toward HER. The *p*-MoS_2/*n*-rGO junction photocatalyst exhibited much better photocatalytic activity than the *p*-MoS_2/undoped-rGO composite. The rGO was transformed from a passive support to an active component of the heterostructure through doping, which was capable of improving all three vital steps in photocatalysis: charge separation, migration, and recombination. The nanoscale *p*−*n* junction positively shifted the onset potential, increased both the photocurrent and the hydrogen evolution rate. The *p*-MoS_2/*n*-rGO heterostructure is a promising photocatalyst, allowing efficient hydrogen production in a wide spectral range from the ultraviolet light through the near-infrared light region. The *p*-MoS_2/*n*-rGO heterostructure contains only earth-abundant, nontoxic, and inexpensive materials. The design principles outlined in this paper can be extended beyond MoS_2 and rGO to enhance the nanoscale heterostructures undergoing development for solar energy conversion.

■ ASSOCIATED CONTENT

Supporting Information

Details on synthesis of materials, photocatalytic and PEC measurements, SEM, TEM, XRD, and IPCE are included in the Supporting Information. This material is available free of charge via the Internet at http://pubs.acs.org.

■ AUTHOR INFORMATION

Corresponding Author

nick.wu@mail.wvu.edu

Notes

The authors declare no competing financial interest.

■ ACKNOWLEDGMENTS

The resource and facilities used in this work were partially supported by NSF (EPS 1003907), the West Virginia University Research Corporation, and the NASA-WV Space Grant Consortium. S. K. Cushing was grateful to the NSF Graduate Research Fellowship (1102689). The use of WVU Shared Facility was appreciated.

■ REFERENCES

(1) Laursen, A. B.; Kegnas, S.; Dahl, S.; Chorkendorff, I. *Energy Environ. Sci.* **2012**, *5*, 5577.
(2) Li, J. T.; Meng, F. K.; Suri, S.; Ding, W. Q.; Huang, F. Q.; Wu, N. Q. *Chem. Commun.* **2012**, *48*, 8213.
(3) Cushing, S. K.; Li, J. T.; Meng, F. K.; Senty, T. R.; Suri, S.; Zhi, M. J.; Li, M.; Bristow, A. D.; Wu, N. Q. *J. Am. Chem. Soc.* **2012**, *134*, 15033.
(4) Meng, F. K.; Hong, Z. L.; Arndt, J.; Li, M.; Zhi, M. J.; Yang, F.; Wu, N. Q. *Nano Res.* **2012**, *5*, 213.
(5) Li, J. T.; Cushing, S. K.; Bright, J.; Meng, F. K.; Senty, T. R.; Zheng, P.; Bristow, A. D.; Wu, N. Q. *ACS Catal.* **2013**, *3*, 47.
(6) Fujishima, A.; Honda, K. *Nature* **1972**, *238*, 37.
(7) Meng, F. K.; Li, J. T.; Hong, Z. L.; Zhi, M. J.; Sakla, A.; Xiang, C. C.; Wu, N. Q. *Catal. Today.* **2013**, *199*, 48.
(8) Li, Y. G.; Wang, H. L.; Xie, L. M.; Liang, Y. Y.; Hong, G. S.; Dai, H. J. *J. Am. Chem. Soc.* **2011**, *133*, 7296.
(9) Lee, J. K.; Lee, W.; Yoon, T. J.; Park, G. S.; Choy, J. H. *J. Mater. Chem.* **2002**, *12*, 614.
(10) Thurston, T. R.; Wilcoxon, J. P. *J. Phys. Chem. B.* **1999**, *103*, 11.
(11) Zong, X.; Yan, H. J.; Wu, G. P.; Ma, G. J.; Wen, F. Y.; Wang, L.; Li, C. *J. Am. Chem. Soc.* **2008**, *130*, 7176.
(12) Xiang, Q. J.; Yu, J. G.; Jaroniec, M. *J. Am. Chem. Soc.* **2012**, *134*, 6575.
(13) Zong, X.; Wu, G. P.; Yan, H. J.; Ma, G. J.; Shi, J. Y.; Wen, F. Y.; Wang, L.; Li, C. *J. Phys. Chem. C.* **2010**, *114*, 1963.
(14) Zong, X.; Na, Y.; Wen, F. Y.; Ma, G. J.; Yang, J. H.; Wang, D. G.; Ma, Y.; Wang, M.; Sun, L. C.; Li, C. *Chem. Commun.* **2009**, *153*, 4536.
(15) Sobczynski, A. *J. Catal.* **1991**, *131*, 156.
(16) Kanda, S.; Akita, T.; Fujishima, M.; Tada, H. *J. Colloid Interface Sci.* **2011**, *354*, 607.
(17) Meng, F. K.; Li, J. T.; Cushing, S. K.; Bright, J.; Zhi, M. J.; Rowley, J. D.; Hong, Z. L.; Manivannan, A.; Bristow, A. D.; Wu, N. Q. *ACS Catal.* **2013**, *3*, 746.
(18) Jiang, B. J.; Tian, C. G.; Fan, Q. J.; Jiang, Z.; Wang, J. Q.; Yan, W. S.; Fu, H. G. *J. Phys. Chem. C.* **2011**, *115*, 23718.
(19) Zhang, X. Y.; Li, H. P.; Cui, X. L.; Lin, Y. H. *J. Mater. Chem.* **2010**, *20*, 2801.
(20) Xiang, Q. J.; Yu, J. G.; Jaroniec, M. *Chem. Soc. Rev.* **2012**, *41*, 782.
(21) Williams, G.; Seger, B.; Kamat, P. V. *ACS Nano* **2008**, *2*, 1487.
(22) Ng, Y. H.; Iwase, A.; Kudo, A.; Amal, R. *J. Phys. Chem. Lett.* **2010**, *1*, 2607.
(23) Guo, J. J.; Li, Y.; Zhu, S. M.; Chen, Z. X.; Liu, Q. L.; Zhang, D.; Moon, W. J.; Song, D. M. *RSC Adv.* **2012**, *2*, 1356.
(24) Mukherji, A.; Seger, B.; Qing, G.; Lu, M.; Wang, L. Z. *ACS Nano* **2011**, *5*, 3483.
(25) Li, Q.; Guo, B. D.; Yu, J. G.; Ran, J. R.; Zhang, B. H.; Yan, H. J.; Gong, J. R. *J. Am. Chem. Soc.* **2011**, *133*, 10878.
(26) Min, S. X.; Lu, G. Q. *J. Phys. Chem. C.* **2012**, *16*, 25415.
(27) Hinnemann, B.; Moses, P. G.; Bonde, J.; Jorgensen, K. P.; Nielsen, J. H.; Horch, S.; Chorkendorff, I.; Norskov, J. K. *J. Am. Chem. Soc.* **2005**, *127*, 5308.
(28) Jaramillo, T. F.; Jorgensen, K. P.; Bonde, J.; Nielsen, J. H.; Horch, S.; Chorkendorff, L. *Science* **2007**, *317*, 100.
(29) Jakob, K.; Chen, Z. B.; Reinecke, B. N.; Jaramillo, T. F. *Nat. Mater.* **2012**, *11*, 963.
(30) Chen, Z. B.; Cummins, D.; Reinecke, B. N.; Clark, E.; Sunkara, M. K.; Jaramillo, T. F. *Nano Lett.* **2011**, *11*, 4168.
(31) Li, M.; Cushing, S. K.; Zhou, X.; Guo, S.; Wu, N. Q. *J. Mater. Chem.* **2012**, *22*, 23374.
(32) Wu, N. Q.; Fu, L.; Su, M.; Aslam, M.; Wong, K. C.; Dravid, V. P. *Nano Lett.* **2004**, *4*, 383.
(33) Stankovich, S.; Piner, R. D.; Chen, X. Q.; Wu, N. Q.; Nguyen, S. T.; Ruoff, R. S. *J. Mater. Chem.* **2006**, *16*, 155.
(34) Coehoorn, R.; Haas, C.; Dijstra, J.; Flipse, C.; Degroot, R. A.; Wold, A. *Phys. Rev. B.* **1987**, *35*, 6195.
(35) Wilcoxon, J. P.; Newcomer, P. P.; Samara, G. A. *J. Appl. Phys.* **1997**, *81*, 7934.
(36) Zhou, W. J.; Yin, Z. Y.; Du, Y. P.; Huang, X.; Zeng, Z. Y.; Fan, Z. X.; Liu, H.; Wang, J. Y.; Zhang, H. *Small* **2013**, *9*, 140.
(37) Gelderman, K.; Lee, L.; Donne, S. W. *J. Chem. Educ.* **2007**, *84*, 685.
(38) Li, X. L.; Wang, H. L.; Robinson, J. T.; Sanchez, H.; Diankov, G.; Dai, H. J. *J. Am. Chem. Soc.* **2009**, *131*, 15939.
(39) Tributsch, H.; Bennett, J. C. *J. Electroanal. Chem.* **1977**, *81*, 97.
(40) Sivula, K.; Le-Formal, F.; Michael, G. *ChemSusChem* **2011**, *4*, 432.
(41) Katz, M. J.; Riha, S. C.; Jeong, N. C.; Martinson, A.; Farha, O. K.; Hupp, J. T. *Coord. Chem. Rev.* **2012**, *256*, 2521.
(42) Tilley, S. D.; Cornuz, M.; Sivula, K.; Gratzel, M. *Angew. Chem., Int. Ed.* **2010**, *49*, 6405.
(43) Sivula, K.; Zboril, R.; Le Formal, F.; Robert, R.; Weidenkaff, A.; Tucek, J.; Frydrych, J.; Gratzel, M. *J. Am. Chem. Soc.* **2010**, *132*, 7436.
(44) Tafalla, D.; Salvador, P.; Benito, R. M. *J. Electrochern. Soc.* **1990**, *137*, 1810.